The Planetary Science Journal, 6:208 (18pp), 2025 September https://doi.org/10.3847/PSJ/adef37

Regionalized Formation and Recycling of New Venusian Crust at Chasmata

Nicholas J. Montiel[1], Luc L. Lavier[2], and Douglas J. Hemingway[2]
[1] Università degli Studi di Padova, Dipartimento di Geoscienze, Via G. Gradenigo n.6, 35131, Padova, Italy; nicholasjohn.montiel@unipd.it
[2] University of Texas Institute for Geophysics, University of Texas at Austin, J. J. Pickle Research Campus, Building 196, 10100 Burnet Road, Austin, TX 78758, USA
Received 2024 August 7; revised 2025 June 20; accepted 2025 July 7; published 2025 September 2

Abstract

Venus and Earth are geologically active in ways distinct from each other. Earth exhibits plate tectonics, where the primary resurfacing mechanism is crust formation along a globe-girdling, extensional tectonic setting in mafic crust, the mid-ocean ridge (MOR). While Venus does not exhibit the key characteristics of plate tectonics, it also possesses a globe-girdling, extensional tectonic setting in mafic crust referred to here as the global rift network (GRN). Despite the macroscale similarities, the two rift systems feature disparate characteristics. Using numerical modeling compared against topographic models from Magellan, we test whether seafloor-spreading-like tectonics under Venusian conditions can reproduce the morphology of individual chasmata along the GRN. The results indicate that the MOR-like seafloor spreading does not occur along most of the GRN, only in unique tectonic environments like that within Artemis Corona. On the other hand, we find that rift-embedded coronae along the GRN have morphologies best explained by excess crustal formation and subsequent densification leading to lithospheric delamination like ephemeral subduction postulated for coronae in previous studies. This suggests that secondary hot spots form between the major plumes under Beta, Atla, Themis, and Phoebe Regios. These minor plumes follow the flow of the upwelling mantle to initiate the formation of rift-embedded coronae along the GRN before becoming inactive when the hot spot dies. Such regionalized formation and recycling of the crust under the influence of mantle plumes is consistent with active geodynamics with limited plate mobility, such as predicted by plutonic-squishy lid, deformable lid, and globally fragmented lid tectonic hypotheses.

Unified Astronomy Thesaurus concepts: Venus (1763); Planetary geology (2288); Lithosphere (928); Tectonics (2175); Plate tectonics (1265); Volcanism (2174)

1. Introduction

1.1. Global Tectonic Style

Despite similar bulk chemical and physical properties, Earth and Venus have divergent geological and climatic histories (e.g., D. L. Lourenço 2023). In contrast to plate tectonics on Earth, Venus has been thought to exhibit a distinct yet enigmatic geodynamic mode since early Soviet and American missions started mapping its surface (e.g., P. Rosenblatt et al. 1994; R. G. Strom et al. 1994; D. L. Bindschadler 1995). Attempts to characterize Venus's geodynamic style vary from models of a stagnant lid, in which the surface is not incorporated into mantle convection and can be considered a single plate (V. S. Solomatov & L. N. Moresi 1996; J. E. Guest & E. R. Stofan 1999); to episodic or catastrophic overturning, in which a stagnant lid regime is periodically interrupted by mass recycling of the crust (R. G. Strom et al. 1994); to recent proposals such as a plutonic-squishy lid, in which magmatic intrusion weakens the lithosphere so that it is broken up into regional-scale blocks that recycle locally and have limited horizontal mobility (D. L. Lourenço et al. 2020), a deformable lid, in which magmatism weakens the crust so that all "plate boundaries" are diffuse and no discrete plates form (J. Tian et al. 2023), or a globally fragmented lid, in which the lithosphere is broken up into regional but strong blocks that have limited mobility but are not necessarily incorporated into mantle convection (P. K. Byrne et al. 2021). Two key processes to understand Venus's tectonic regime are the formation and recycling of the planet's crustal layer. Basilevsky proposed that Venus exhibits subparallel, crust-generating spreading centers distributed in the northern hemisphere (A. T. Basilevsky 1992), but later Magellan imagery showed these structures to be inconsistent with Earth-like spreading centers because of what are interpreted to be thrust faults at their boundaries (e.g., S. Hanmer 2023). Even still, analysis of admittance for Venus suggested that the volcanic plains were a younger and potentially more active tectonic regime than the highlands (e.g., M. Simons et al. 1994). After Magellan, this picture was complicated by the random distribution of craters on Venus's surface, suggesting a catastrophic overturn model in which all or most of Venus's crust subducted into the mantle and was replaced with a new crust ~500 Ma. In this scenario, the lithosphere is believed to have since remained stagnant (G. G. Schaber et al. 1992; C. C. Reese et al. 2007). However, recent analysis of the cratering record by R. R. Herrick et al. (2023) shows that the random distribution could also be explained by a sequence of regional, stochastic resurfacing events and not a global overturn of the crust. Modeling of lithospheric structure based on topography and gravity suggests that Venus's mafic crust is ~20–25 km thick, much thicker than the equivalent oceanic crust on Earth, and that the lithosphere is relatively thin at ~95 km (e.g., F. S. Anderson & S. E. Smrekar 2006; A. Jiménez-Díaz et al. 2015). The presence of an asthenosphere is debated (E. Mulyukova & D. Bercovici 2020), but modeling suggests a low-viscosity layer produced by partial

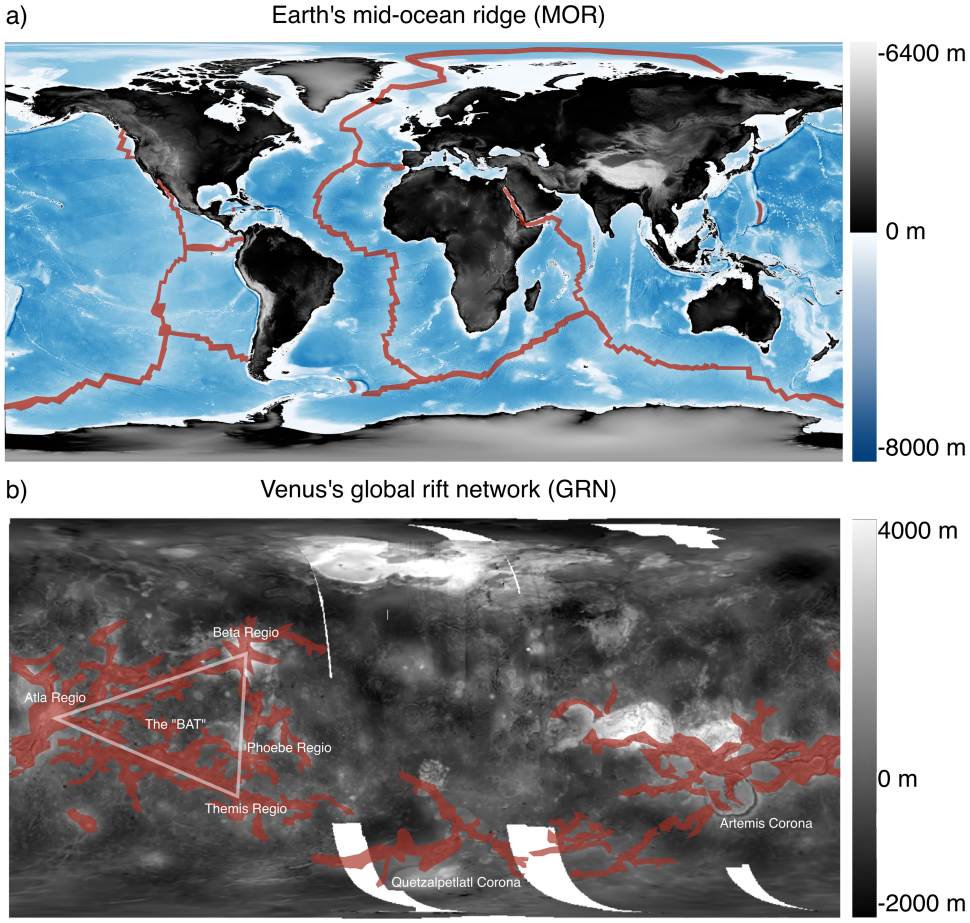

Figure 1. (a) A topographic and bathymetric map of Earth with the major segments of the MOR highlighted in red. (b) A topographic map of Venus with the GRN highlighted in red. Major geographic features that the GRN links between are labeled, including the BAT region, which is outlined in white. Unlike the MOR, the GRN is discontinuous, sinuous, and made up of many subparallel branches that radiate out from or link between major volcanic rises and large coronae. Despite this, both are global, extensional tectonic settings that are some of the youngest features on their planets. Venus's rift distribution is based on the work of A. S. Krassilnikov et al. (2012). Imagery from Jesse Allen, NASA's Earth Observatory, using data from the General Bathymetric Chart of the Oceans produced by the British Oceanographic Data Center and from ACT-REACT Quickmap.

melt in the mantle (similar to Earth's asthenosphere) from ~80 to 315 km (J. S. Maia et al. 2023).

Photogeology from Magellan and other spacecraft shows a planetary surface with diverse landforms that suggest recent active volcanism and tectonism (S. E. Smrekar et al. 2010; E. Marcq et al. 2013; E. V. Shalygin et al. 2015; R. R. Herrick & S. Hensley 2023). This raises the possibility that Venus's crust could have been formed and recycled in the geologically recent past. Earth's surface is 71% oceanic crust formed by volcanic intrusion and extrusion along a global rift system: the mid-ocean ridge (MOR; e.g., R. Searle 2013). The MOR is bounded by normal faults and exhibits an axial, linear volcanic zone that is continuous, narrow, and linear except where displaced by transform faults between rift segments that significantly offset the MOR (Figure 1(a)). This oceanic lithosphere is then migrated thousands of kilometers away to be recycled at subduction zones. While Venus seemingly does not have an MOR or global subduction zones, it does have its own global extensional system that shares important similarities and differences with the MOR on Earth.

Both the global rift network (GRN) and MOR are extensional tectonic environments that are global systems, some of the youngest features on their respective planets (S. E. Smrekar et al. 2010; R. R. Herrick & S. Hensley 2023; R. R. Herrick et al. 2023), and both form in mafic volcanic-tectonic settings. On the other hand, Venus's GRN (Figure 1(b)) is made up of discontinuous, branching, and sinuous rift segments (also referred to as chasmata) that are subparallel to each other and connect volcanic provinces. For instance, the Beta–Atla–Themis region (BAT) is comprised of three large volcanic edifices connected by the Zverine, Hecate, Devana, Rona, and Parga Chasmata rift systems (L. S. Crumpler et al. 1993; M. A. Ivanov & J. W. Head 2011; M. W. Airey et al. 2017). Another major difference between the MOR and the GRN is that individual rift segments on Venus show limited stretching of the lithosphere (<100 km of extension compared to thousands of kilometers for segments of the MOR; E. R. Stofan et al. 1989). Previous analysis of Venusian hypsometry and the topography of chasmata suggests that they are distinct from MORs and rift systems on Earth, with the possible exception of ultra-slow-spreading centers like the Gakkel Ridge or the South West Indian Ridge (P. R. Stoddard & D. M. Jurdy 2012). However, no modeling work has demonstrated whether seafloor spreading under Venusian conditions would form structures like MORs on Earth. Additionally, no global subduction zones are observed on Venus, but the troughs that surround Artemis and Quetzalpetlatl Coronae have been hypothesized to be examples of regional subduction with back-arc extension occurring in the upper plate

(e.g., A. Davaille et al. 2017; A. J. Gülcher et al. 2020). These possible subduction zones only occur around particularly large corona and are not present along the entire GRN, precluding their role in accommodating crustal formation via spreading by recycling older crust into the mantle. These observations suggest that if processes of crustal formation and subduction occur on Venus, they are limited to certain regions and are not global processes.

If the GRN is analogous to the MOR, in other words an example of how spreading centers would evolve differently under Venusian thermomechanical conditions, and if crustal recycling is regionalized on Venus, then the GRN should be a place where crust is formed and recycled. In that case, features similar to suduction zones should be colocated with extensional systems on Venus.

2. Methods

Numerical modeling is crucial for understanding processes and temporal evolution since in situ and remote sensing geology largely provide "only" snapshots in deep time. Determining how to link apparently disparate geological features and landscapes along evolutionary pathways requires numerical modeling, despite the inherent limitations and simplifications of simulations (e.g., W. R. Buck et al. 2005; L. L. Lavier & G. Manatschal 2006; N. J. Montiel et al. 2023). With regard to the GRN and associated rifts and coronae, this provides a means to identify the morphologies of rifts under controlled conditions and to compare those morphologies to rifts and coronae on Venus. To predict the morphological regimes that result from crustal formation, we use the software package Fast Langrangian Analysis of Continua (GeoFLAC; e.g., L. L. Lavier & G. Manatschal 2006; A. E. Svartman Dias et al. 2015; N. J. Montiel et al. 2023). GeoFLAC has been used to model terrestrial rift and subduction systems for three decades and is useful for studying the rheological, thermal, kinematic, and petrological development of tectonic systems. It is a 2D, explicit, Lagrangian code that includes elastoplastic and viscoelastic behavior of materials (P. A. Cundall 1987; A. N. B. Poliakov et al. 1993).

2.1. Model Setup

Venusian initial conditions result in unique rift behaviors (A. J. Gülcher et al. 2023; A. Regorda et al. 2023; A. J. P. Gülcher et al. 2024), and approximating that environment requires unique boundary conditions for GeoFLAC. We set the surface temperature to 475°C (representing the surface temperature at the lowest elevations), the surface pressure to 9.3 MPa, and the gravitational acceleration to 8.9 m s^{-2} (A. Regorda et al. 2023). Surface heat flow is set as a free boundary on top, and thermal conditions on the bottom are determined by the adiabatic geotherm (0.003°C km^{-1}) and mantle potential temperature (1400°C). The geothermal profile between is determined by constitutive equations of heat flow and a prescribed thermal anomaly (N. J. Montiel et al. 2023). The depth of the lithosphere-asthenosphere boundary (LAB) is defined as the 1300°C isotherm, which varies depending on initial surface heat flow. Isostatic equilibrium is maintained in the model via a Winkler foundation, where compensation depth is assumed to be the bottom boundary. Flexural responses to loading and unloading are calculated using elastic and viscoelastic constitutive updates (e.g., P. A. Cundall 1987; A. N. B. Poliakov et al. 1993). We model an initially 20 km thick basalt crust based on topographic and gravity data as well as previous 2D rifting and models (e.g., P. B. James et al. 2013; A. Jiménez-Díaz et al. 2015; A. Regorda et al. 2023). Extension is imposed by velocity boundary conditions on the left and right sides. The generation of new crust is similarly prescribed by creating columns of new material at the model's center from the base of the basaltic crust to the surface to a minimum of 3 km deep; it is not modeled to be a result of melt production and crystallization so that we can control the relative rates of extension and crust formation, though latent heat is accounted for. If extension does not create enough accommodation space, the excess of new material accumulates at the top and bottom of the expanding column. This approach is identical to the method used by W. R. Buck et al. (2005) for the study of slow- and fast-spreading MORs.

In the case where the crust thickens due to the vertical expansion of the column, we need to consider the role of high-density phase changes such as eclogitization, partial eclogitization, and granulitization. Eclogitization, the formation of garnet-omphacite in the mafic crust, requires high pressure and temperature, and the process is much faster in hydrous conditions (e.g.,M. L. Leech 2001; E. Duesterhoeft et al. 2014). On Earth, eclogitization is crucial for creating slabs dense enough to drive subduction and is thus the driving force behind plate tectonics (e.g., D. Forsyth & S. Uyeda 1975; C. P. Conrad & C. Lithgow-Bertelloni 2004; W. P. Schellart 2004). On Venus, the role of eclogitization has been unclear. Studies show that, at Venus's lower lithostatic pressures relative to Earth, eclogite forms deeper and at smaller volumes to result in a total lack of global subduction to drive mobile lid tectonics (S. R. Taylor & S. McLennan 2008; J. Chen et al. 2022). However, the temperature conditions that prevail for extensional tectonic and hot-spot settings may be conducive to eclogitization at shallower levels of the lithosphere. The higher surface temperature (∼470°C, varying with altitude) results in an elevated thermal profile relative to Earth that can cause eclogite to form more shallowly on Venus, especially during mantle upwelling. This is further enhanced on Venus because it has a thicker basalt crust (∼25 km) than on Earth (∼6 km; S. R. Taylor & S. McLennan 2008; A. Regorda et al. 2023; S. E. Smrekar et al. 2023); therefore, eclogitization can occur deeper than it could in rift settings on Earth if thermal conditions were sufficient for it.

Partial eclogitization and granulitization also need to be considered, since the transition from basalt to eclogite is not linear or discrete, but progressive. Granulite is a high-grade metamorphic facies-dominated plagioclase, orthopyroxene, and garnet while lacking in muscovite and hydroxyl-bearing silicates; it forms at greater than 700°C and between ∼0.7 and 1.3 GPa (A. J. R. White 1964; S. L. Harley 1998). Partially eclogitized outcrops where eclogite and granulite facies are mixed have been observed at Holsnøy in the Bergen Arc of Norway, as well as other localities, and are a result of gradual and inhomogeneous metamorphic reactions in anhydrous settings. These complex phase changes result in a ∼10% density increase from the basalt protolith (H. Raimbourg et al. 2007).

To model the phase transitions from basalt to higher-density phases, we start with the eclogite phase curve derived from Venera 13 and 14 and Vega 2 X-ray spectrometry by J. Chen et al. (2022) to simulate phase transformation from intrusive

Table 1
Summary of the Rheological and Creep Parameters Used for Our Numerical Modeling Experiments

Parameter	Mantle	Basalt	High-temperature Mantle Shear Zones	High-density Phase ("Eclogite")
Density (kg m^{-3})	3300	3000	3300	3450
Creep exponent, n	3	3.05	3	3.5
Creep pre-exponent (MPa^{-n} s^{-1})	7.00E+04	1.25E–01	3.00E–06	1995.26
Creep activation energy (kJ mol^{-1})	520	376	300	403
Friction angle (deg)	30	30	30–15	30
Cohesion (MPa)	44–4	44–4	44–4	40–4
Lamé parameter, λ (Pa)	6.70E+10	7.80E+10	6.70E+10	7.00E+10
Lamé parameter, μ (Pa)	6.70E+10	6.70E+10	6.70E+10	7.00E+10
Work and energy thresholds (J)	5.00E+07	…	…	…
	Depth < 10 km, $T < 400$°C	…	…	…
Thermal conductivity (W mK^{-1})	3.3	3.3	5	3.3–5.7

Note. We used the same creep laws and rheological parameters as in N. J. Montiel et al. (2023) but without serpentinite, felsic crust, low temperature, and crustal detachment faults and with the addition of high-density phases. The parameters for eclogite were taken from J. Zhang & H. W. Green (2007). High-temperature shear zones are treated in the same manner as in Table 1 of N. J. Montiel et al. (2023).

basalt to eclogite at the base of the Venusian crust. The rheological characteristics for eclogite are derived from J. Zhang & H. W. Green (2007). We extend the densification range beyond regular eclogite phase curves to account for partial granulitization and eclogitization so that phase changes can occur at lower depths and shallower pressures, from a minimum depth of 25–40 km, respectively. Granulite can form at depths as shallow as 15 km in regions with an elevated geotherm (S. Earle 2019, chapter 7). The phase transition in the model is instantaneous to reflect the rapidity of change on geological timescales, so we split the difference between the minimum depth of granulitization and eclogitization. The resulting curve is a piecewise function: $z = -625T + 450,000$ for less than 600°C and $z = -117T + 145,000$ at greater temperatures, where T is temperature (°C) and z (m) is the depth at which high-density phases form for temperature (τ). It is worth noting that the behaviors of eclogite and other high-density phases in a truly dry mantle are relatively unconstrained because Earth's water-rich mantle dominates the literature on the subject (e.g., T. Tsujimori & C. Mattinson 2021). In addition, the volatile content of Venus's mantle, whether water, carbon dioxide, or sulfur, is unknown (S. E. Smrekar & C. Sotin 2012). Therefore, the actual processes behind and behaviors of high-density phase transitions in Venus's interior are an open question, hence the decision to generalize phase changes as granulitic and eclogitic with a low-pressure and high-temperature extension of the phase curve. For other lithologies (basaltic crust, olivine mantle, and high-temperature shear zones), we use the rheology and methodology as described in N. J. Montiel et al. (2023, Table 3.1) with additions (Table 1).

2.2. Parameter Space

Because plate tectonics, and therefore slab pull, is absent on Venus, the main potential drivers of tectonic motion on Venus are plume push, ridge push, and mantle drag (S. E. Smrekar et al. 2018). This puts an upper limit on the extension rates of $\sim$1 cm yr^{-1} (D. Forsyth & S. Uyeda 1975). The lower end of the estimates for extension rates is based on calculations of tectonic strain rates from crater deformation on Venus (R. E. Grimm 1994), which suggests that Venus has tectonic rates of 0.01 cm yr^{-1} (2 orders of magnitude less than on Earth). For the purposes of modeling, we prescribe extension rates of 1, 0.1, and 0.01 cm yr^{-1} for the left and right boundaries. The prescribed rate of crustal formation is varied over the same range to model the resulting morphologies of magma-starved, magmatic, and supermagmatic extension. Another parameter that we vary is initial surface heat flux. Estimates of surface heat flow on Venus carry a lot of uncertainty since it cannot be measured directly. Recent estimates of heat flux based on elastic thickness suggest a value of 101 ± 88 mW m^{-2}, allowing for a wide range of possible thermal regimes (J. G. O'Rourke & S. E. Smrekar 2018; S. E. Smrekar et al. 2023). Combined with the high surface temperatures, this can produce geothermal gradients ranging from 5°C km^{-1} to 30°C km^{-1} or even higher at shallow depths (R. Ghail 2015). When consideration is given to the presence of carbon dioxide in the mantle, this results in high degrees of partial melting (a possible origin for the Venusian asthenosphere), a crust that is deformationally decoupled from the mantle, and a thin lithosphere (R. Ghail 2015). We chose two conservative values for initial heat flux at 50 and 80 mW m^{-2} representing the low-middle and middle parts of the estimated range of possible surface heat flows. We ignore the high end of the range because it far exceeds the background heat flow for tectonic settings on Earth (e.g., J. H. Davies 2013) and the lowest end because we expect that to be a tectonically quiescent setting. A shallowing of the LAB following a Gaussian curve is implemented for cases with thick lithospheres; for thin lithospheres, a thicker, and therefore weaker, crust is implemented to ensure that deformation is localized at the center of the model.

2.3. Topographic Comparisons

The modeled rift topography needs to be compared with the observed topography of rift segments along the GRN. The topographic and gravity data we use are taken from M. A. Wieczorek (2015). We pick rift segments that are structurally similar along the strike (to reduce error and noise) as well as rift-embedded coronae along the GRN. For each rift segment selected, we trace a path down the rift's axis and take orthogonal topographic profiles across the axis every 5 km. The length of each profile is 200 km for rifts. When topography is plotted as a surface centered on the traced rift axis, it has the effect of "straightening out" the rift to further reduce noise and make the fundamental characteristics and

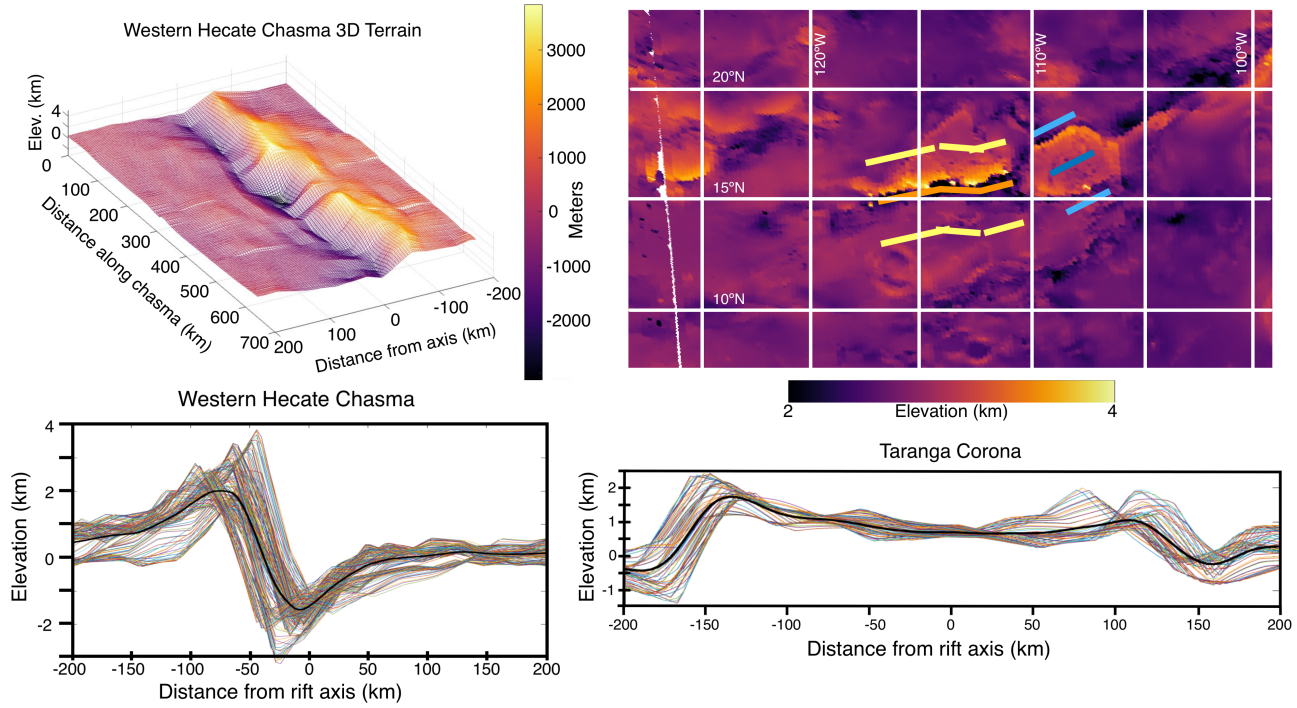

Figure 2. Hecate Chasma and Taranga Corona as examples of how individual rift segments and coronae are analyzed. In the top right panel, the orange line traces out the rift axis of Hecata Chasma, while the yellow lines 200 km to either side are the endpoints of topographic transects taken every 5 km along the rift axis. The dark blue and light blue lines do the same, respectively, for Taranga Corona. The top left panel shows the surface topography constructed by adjacent profiles centered on the outlined rift axis. This has the effect of straightening out the rift and reducing noise for the aggregated (colored lines) and averaged (black bold line) topography (bottom left panel). The topographic profiles in the bottom right panel show the same for Taranga Corona. Map image from ACT-REACT Quickmap.

structure of the rift clear. For rift-embedded coronae, the length of the profile varies to give at least a 50 km margin on either side of the corona. The central axes across which the profiles trend are much shorter for coronae as well. Both the mean topographic profile and the individual profiles in bulk are analyzed (Figure 2).

We selected 56 rift segments along the GRN to produce figures like those shown in Figure 2 and categorized them according to their topography and how they compared to different kinds of model topographies (Table A1). The basis for comparison between the models and the observations is the topography and morphology of both. Each rift segment is categorized based on a preponderance of diagnostic features, such as (1) the width of the rift; (2) the depth of the rift; (3) the elevation of the epaulements (or rift flanks) compared to the undeformed background; (4) the symmetry or asymmetry of a rift, including the relative heights of epaulements or a gentle slope from epaulement to rift floor; (5) the presence or absence of an axial ridge or axial valley; (6) the presence or absence of troughs that bound a rift-embedded corona; (7) the presence or absence of a central peak in a rift-embedded corona; and (8) the presence or absence and shape of an interior plateau for rift-embedded coronae. If a particular model regime and a particular rift segment share diagnostic features between them, they are characterized as analogous. Certain categorizations are associated with model regimes, as explained below.

3. Results

3.1. Model Regimes

We performed 18 different numerical modeling experiments with GeoFLAC that show varied patterns of topography and geodynamics. Some share similarities with real topography, others do not, and some are ambiguous. Surface heat flow does not seem to significantly affect rift or corona evolution in our models. High extension rates may cause a higher degree of asymmetry due to stochastic variations in rift initiation. Broadly, the morphology and structure of the modeled cases fall into four families or regimes that are controlled by the relative rate of crustal addition to the rate of extension (Figure 3).

3.1.1. Overthickening Regime

In scenarios where the extension rate is substantially lower than the rate of crustal addition, new crust is unable to be accommodated by spreading, and the crust thickens as a result (Figure 4). The upwelling of the asthenosphere due to far field extension combined with the thickened root pushes basalt into the *P–T* conditions necessary for phase transitions. Because the metamorphosed phase is denser and weaker than basalt and the olivine mantle, the dense roots may drip into the mantle. Surface expression of this process starts with the initial creation of a topographic high surrounded by a trough produced by flexure of the lithosphere. Following the collapse of the dense root into the mantle, the topography inverts to create a bowl-shaped plateau. The diagnostic topography associated with this regime is an internal plateau, plateau rims, and boundary troughs. In some cases, the plateau is up to 2 km above the surrounding plain, while in others, the plateau is nearly level with the surrounding plains. Separating the plateau from the undeformed surroundings are elevated rims and then a trough further out. Unlike the troughs in the initial phase, these correlate to where the crust is delaminating into the mantle. Dynamically, the diagnostic characteristics are the

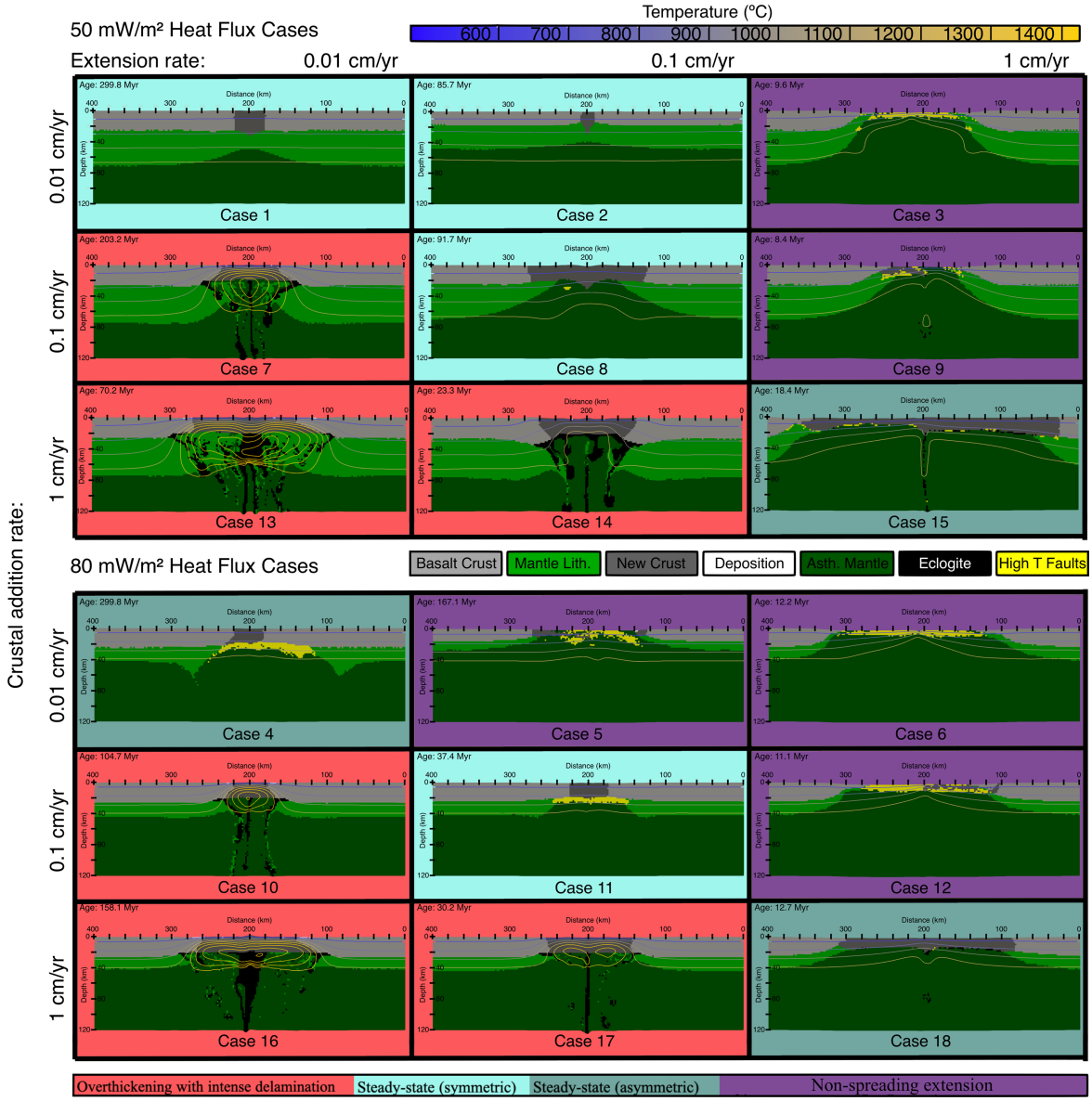

Figure 3. Overview of numerical modeling experiments, showing how structural regimes vary due to their location within our parameter space. The top panel shows the nine cases run at an initial surface heat flux of 50 mW m^{-2}, with each column representing a different extension rate (0.01, 0.1, and 1 cm yr^{-1}) and each row representing a different rate of crustal addition to simulate spreading (same range of values). The bottom panel shows the same but for an initial surface heat flux of 80 mW m^{-2}. The background color of each inset codes for the four modeling regimes: red for overthickening crust; light blue and dark blue for symmetric and asymmetric pseudospreading, respectively; and purple for nonspreading (classical rift with little new crust being generated). Within each model, contour lines show temperatures (isotherms from 600°C to 1400°C with intervals of 200°C), and colors show phases (gray for basalt crust, dark gray for newly generated basalt crust, green for lithospheric mantle, dark green for initially asthenospheric mantle, black for dense phases, yellow for high-temperature shear zones/detachment faults formed via damage rheology, and white for sedimentary/volcanic deposition). It is important to note that the asthenospheric mantle that becomes part of the lithosphere during thermal evolution does not change its initial color.

thickening of the basalt crust and the dripping of dense phases into the mantle at the edges of the section of thickened crust.

A key feature of this regime is the emergent dynamics caused by densification via phase change. Initially, the dense root forms at the center of the model where crust is being added. When that root collapses, it drags the surrounding basalt crust behind it such that it also metamorphoses into eclogite and other dense phases as it crosses the phase transition in *P–T* space. It also opens a hole in the center of the rift in which the olivine asthenosphere upwells to replace the metamorphic root. These two processes combine to create a system of "phantom subduction," where the remaining parts of the metamorphic root on either side of the lithospheric hole collapse into the asthenosphere while pulling in new basalt from outside the widening rift to transform into dense phases, continuing the cycle. While there is no slab, this is dynamically similar to trench rollback and exerts a pull on the lithosphere. When comparing this model regime to the observations, the overthickening regime is its own category like the pseudospreading regime and unlike the nonspreading regime, as seen below.

3.1.2. Pseudospreading Regime

When the extension rate and the rate of crust formation are roughly equal, the accommodation space created by rifting is

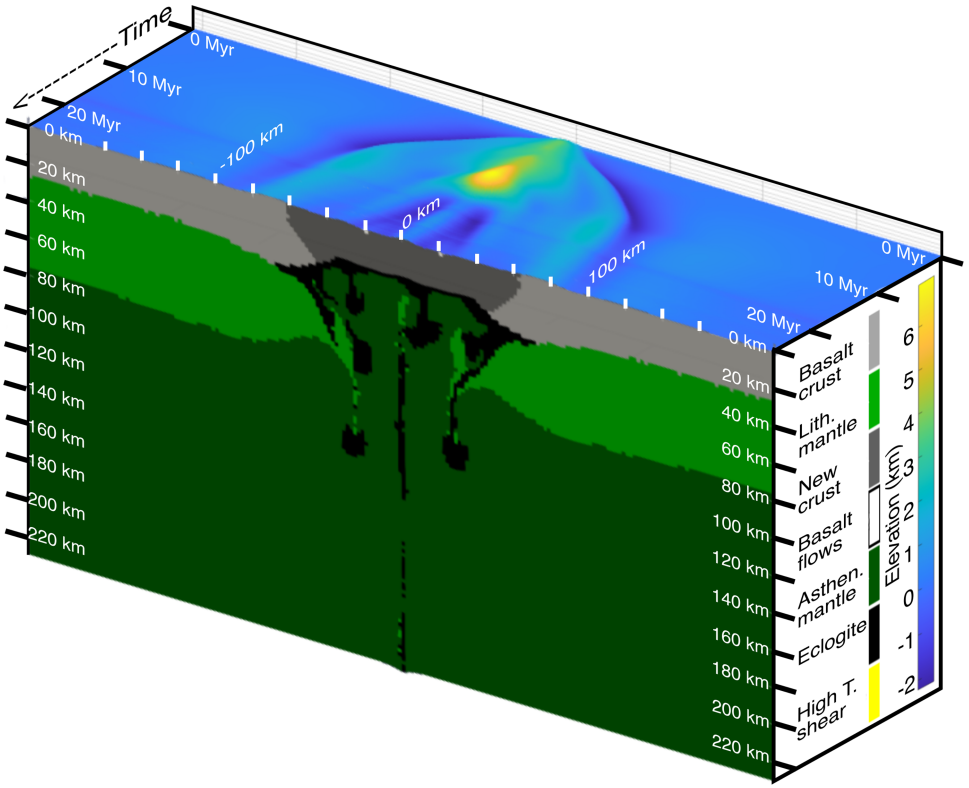

Figure 4. A pseudo–block diagram showing an example of the overthickening regime (model case 14 at 50 mW m^{-2} heat flux, 0.1 cm yr^{-1} extension rate, and 1 cm yr^{-1} addition rate). The face shows the structure of the 2D model at 23.3 Myr, the end of the model's run. The top shows the topographic evolution through time by stacking 2D topographic profiles side by side. This shows how the overthickening regime is characterized. Structurally, overthickening produces an unstable, dense root that drips and delaminates from the crust into the mantle. Topographically, the thickening crust creates a broad mountain surrounded by a flexural trough that then inverts as high-density phases collapse into the mantle. The trough persists, though it is maintained dynamically by the delaminating root.

filled by new crustal material in a steady state that maintains a stable crustal thickness. This results in either a complex, wide, asymmetric rift (Figure 5(a)) or a symmetric rift zone along the pseudospreading axis (Figure 5(b)). While not shown as a separate phase in Figure 2, new lithosphere is also formed as the previously asthenospheric mantle upwells and cools, as the LAB depth is determined by the geothermal profile. Diagnostic characters for this regime are diverse, but the key topographic features are a narrow (<40 km) and deep (>1 km) axial rift for the symmetric regime and a ridge bifurcating two differently elevated plains regions within a wide rift with a complex system of ridges and faults for the asymmetric case. While there may be minimal amounts of densification and lithospheric dripping, they do not control the overall structure. The overall structure is instead controlled by the rate of extension and the localization of deformation with respect to the location of crustal generation/dikes. Similar studies of MORs on Earth (W. R. Buck et al. 2005) indicate that strain tends to localize away from where new crust is being accreted to either plate. The result is asymmetric accretion along the MOR, producing a thinner crust on one side than on the other. This is also consistent with observations of asymmetric growth at MORs like the East Pacific Rise, where up to 70% of new crust has been added to the Nazca plate, with the remainder accreted to the Pacific plate at various stages throughout its history (e.g., R. D. Müller et al. 1998). When each rift segment is categorized based on its diagnostic features, asymmetric and symmetric pseudospreading are categories unto themselves.

3.1.3. Nonspreading Regime

In cases where the extension rate is greater than the rate of crustal addition, little or no new crustal material fills the accommodation space. As a result, the mantle is exhumed to the surface along high-temperature detachment faults and takes on a similar morphology to that of classical rift valleys (Figure 6). While the model technically shows a case of hyperextension where the crust thins to zero and ductile deformation is occurring at the surface, this is unrealistic for Venus since we are purposefully starving crustal addition. Instead, we use this regime as a proxy for nonspreading rifts. Because only limited amounts of new crust are being generated to fill the accommodation space, this model regime produces graben and half-graben structures akin to continental rifting or aulacogens on Earth. This regime is generally characterized by a deep and flat rift floor with one or two slightly elevated epaulements (<300 m, approximately, above the surrounding plain). The rift walls are generally steep but can be gentle if they are the upper block of a half-graben. On the rift floor, there is sometimes an axial valley that represents where the model adds new crust, though in nature, this feature should be erased by volcanism and dynamic topography. Importantly, the rift widens at the same rate as extension. Together, these diagnostic features allow the nonspreading regime to act as a test for the null hypothesis that a given rift segment is not experiencing seafloor-spreading-like tectonism. Therefore, when analyzing and categorizing individual rift segments, this regime is represented by the graben and half-graben categories.

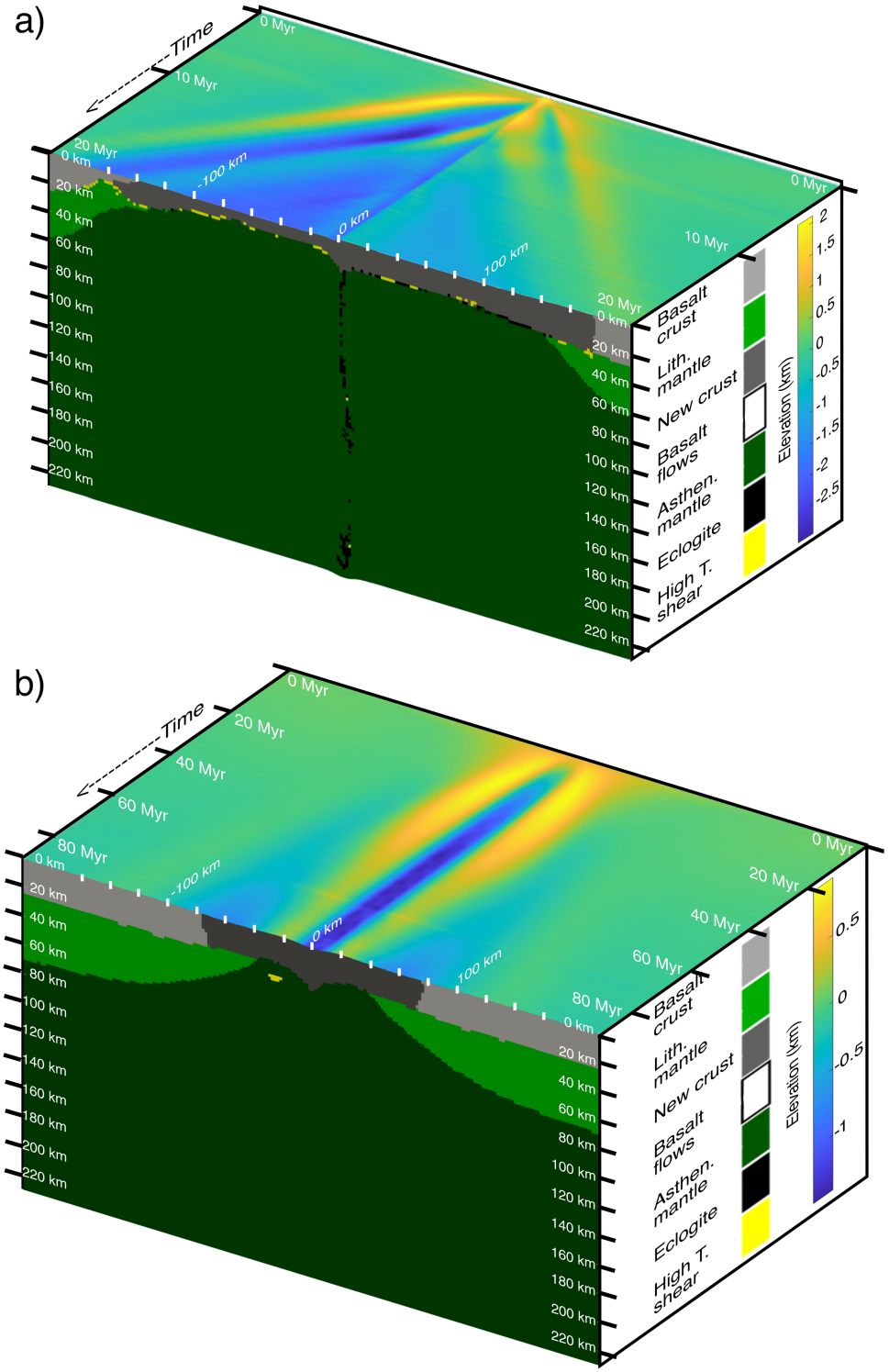

Figure 5. (a) A pseudo–block diagram showing an example of an asymmetric pseudospreading regime (model case 15). This shows some of the characteristics of this regime: differing crustal thickness on either side of the rift axis, a wide rift with multiple ridges along its length, and an axial ridge–valley system. (b) A pseudo–block diagram showing an example of a symmetric pseudospreading regime (model case 8), with the diagnostic axial valley and raised epaulements.

3.2. Topographic Comparisons

Using the diagnostic features described above, we find that of the 56 rift segments analyzed, only six rift segments from three chasmata are consistent with an MOR-like spreading center. Most of the chasmata we analyzed do not share a preponderance of diagnostic features with either the symmetric or asymmetric pseudospreading regime (Figure 7(a)). Based on their topography, the majority of rift segments on Venus are either full grabens or half-grabens. For example, Hecate Chasma's east and west segments (separated by Taranga Corona) exhibit one higher epaulement with an elevation of 1.5–2 km and a rift floor that is 1–2 km deep. The other flank is gently sloped and simply grades from the surrounding plains. These features indicate half-graben-style rifts, with one major boundary fault with many minor faults.

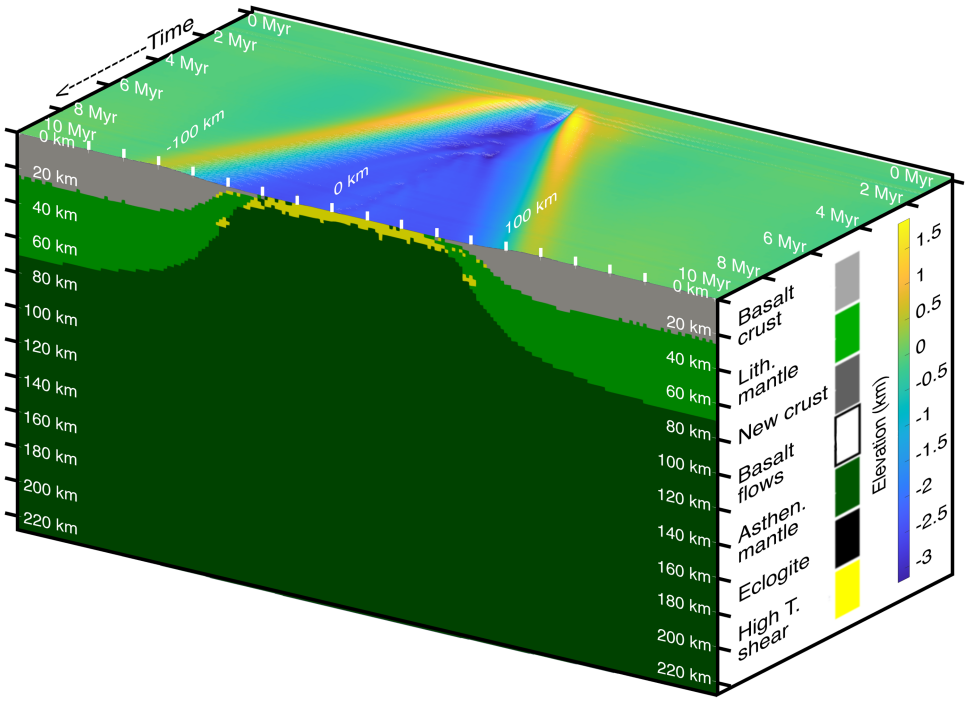

Figure 6. A pseudo–block diagram showing an example of the nonspreading modeling regime (model case 3), with these diagnostic features: widening rift, slightly elevated flanks, deep rift floor, little new crustal addition, and gentle slopes to the rift floor.

A similar analysis applies to other chasmata. Individual segments of Parga, Quilla, Diana, Devana, Dali, and other chasmata are half-grabens or exhibit a complex morphology that shares few if any diagnostic features with either pseudospreading model regime.

There are two observed rift systems in this analysis that exhibit similarities with the pseudospreading regime, the most illustrative being the Britomartis–Bonnevie system within Artemis Corona (Figures 3 and 7(b)). Britomartis Chasma runs from NE to SW from the outside to the center of Artemis Corona and is divided into three linear rift segments separated by lateral offsets, like the transform faults at an MOR. The northern segment of Britomartis Chasma possesses a ridge along the rift axis, with broad depressions on either side with different depths. This is consistent with some examples of the asymmetric pseudospreading regime, especially model case 15 (Figure 7(b)). The central segment of Britomartis is difficult to categorize because it is relatively short and complex, but the southern segment shares important characteristics with symmetric pseudospreading models. It is composed of two parallel ridges along the rift axis, with an axial valley between the two that has a floor at the same elevation as the surrounding plains, like model cases 1, 2, and 8. However, the scale of southern Britomartis is larger than that of the models, with an elevation of nearly 2 km compared to the modeled topography of only a few hundred meters. This discrepancy may be explained by dynamic topography and volcanic processes that our models do not capture. In the southwestern portion of Artemis, Britomartis Chasma makes an approximately 110° turn to the right and then irregularly curves 180° to the left around an enigmatic tectonic province of which the most prominent feature is Bonnevie Crater. This "Circum-Bonnevie" Chasma has morphology that is consistent with spreading along its length, such as the presence of axial ridges and axial valleys.

As described above, the nonspreading regime works as a null-hypothesis test because it shows very little crustal addition and is comparable with graben and half-graben rifts on Earth (W. S. Kiefer et al. 2024). Some of the largest rifts on Venus are comparable to this family of models (Figure 8). The portion of Devana Chasma south of Beta Regio is a good example of this. Devana Chasma shares the diagnostic traits of the nonspreading regime, such as a wide, flat rift floor with steep sides and epaulements elevated by only a few hundred meters. A similar geometry exists for Ralk-Umgu, Quilla, Rona, and other chasmata. Apparent half-grabens such as Dali and Hecate Chasmata, along with individual segments of Quilla, Parga, and Devana Chasmata, match closely to asymmetric cases of nonspreading, such as model case 12. For most rift segments along the GRN, models showing little to no crustal addition instead of a Venusian equivalent to seafloor spreading are the most consistent with topographic and morphological observations.

While comparisons between pseudospreading with observed rift topography fall short and comparisons with nonspreading systems suggest a lack of crustal generation along most of the GRN, the overthickening regime shows strong similarities with coronae in and around chasmata (Figure 9). The characteristic topographic inversion associated with the collapse of the dense root that produces an interior plateau is observed at many of the coronae considered here. In addition, the boundary troughs maintained by delaminating crust are also observed, as are corona rims. The best examples of these similarities are between model cases 14 and 13 and Atahensik, Atate, Miralaidji, and Taranga Coronae. Miralaidji comparisons are more tenuous since it lacks the bowl-shaped profile across its interior plateau, but it does share the central peak seen in many models, including model case 13.

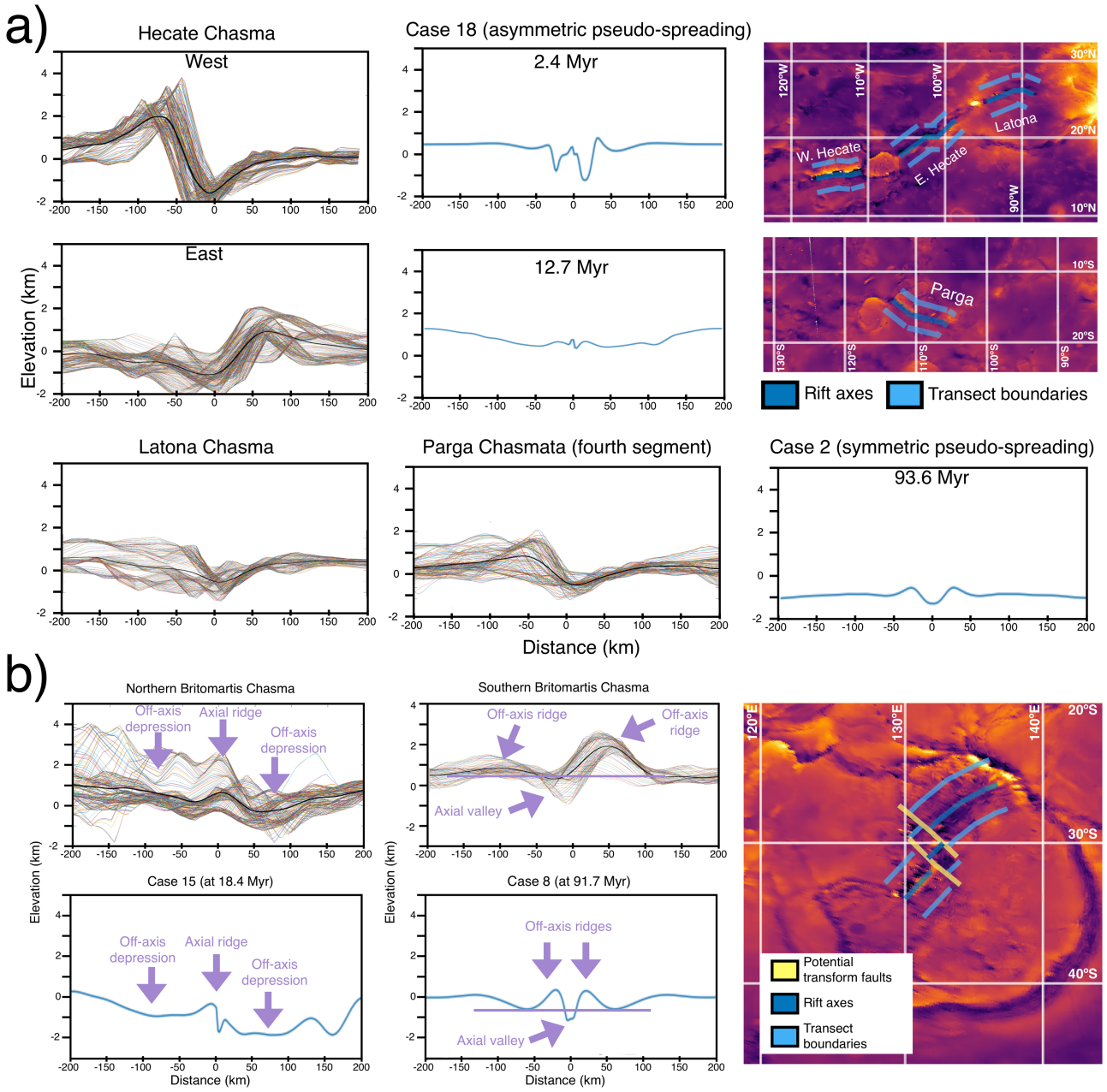

Figure 7. (a) Cross sections of Hecate Chasma (east and west segments), Latona Chasma, and part of Parga Chasmata along with model topography from model case 18 (at 2.4 and 12.7 Myr) and model case 8, showing the difficulty of matching diagnostic features between modeled and observed topography, indicating that pseudospreading is unlikely for most rifts on Venus. Map insets show the location and geographic context of the aggregated and averaged topographic profiles. Dark blue and orange lines trace out the rift axes, while light blue and yellow lines mark the boundaries of each topographic transect/profile. (b) Cross sections of northern and southern Britomartis Chasma compared to model cases 15 and 8 to show examples of matching diagnostic features. It is important to note that Britomartis lies within Artemis Corona (right map panel) and is therefore part of a unique tectonic environment on Venus. Dark blue lines trace out the rift axes, light blue lines mark the boundaries of each topographic transect/profile, and yellow lines trace out the potential transform faults in Britomartis Chasma.

4. Discussion

4.1. Character of the GRN on Venus

The pseudospreading models do not share key diagnostic characters with individual chasmata within the GRN, except for the unique cases of Britomartis Chasma and northern Devana Chasma. For symmetric pseudospreading, MOR-like morphology should be apparent along the GRN. At Venus's predicted tectonic rates (0.01–0.1 cm yr^{-1}; R. E. Grimm 1994), relatively symmetric and slow-to-intermediate spreading centers are expected. However, most of the observed chasmata in this study do not exhibit a linear mountain chain or ridge with a deep axial valley that is characteristic of the pseudospreading model regime or slow-to-intermediate MORs on Earth (e.g., R. Searle 2013). Along the branch of the BAT system between Beta and Atla Regios, the rift segments have the topographic profiles of half-grabens, alternating in vergence between segments.

The dominant form of extension on Venus is not through half-graben rifts but full graben rifts (e.g., A. Foster & F. Nimmo 1996; P. K. Byrne et al. 2021; S. Hanmer 2023; W. S. Kiefer et al. 2024). Of the 56 rift segments analyzed in this study, the majority of interpretable chasmata consist of full graben structures along their length and are consistent with the

Figure 8. Cross sections of Southern Devana, Ralk-Umgu, Dali, Quilla, and unnamed chasmata compared to model cases 12, 3, and 5 to show shared diagnostic features between the nonspreading regime and representative rift segments on Venus. Interpretation is based on the presence and elevation of epaulements relative to the rift floor and the surrounding plains as well as the shared widths and depths of chasmata and modeled rifts. Map insets show the location and geographic context of the aggregated and averaged topographic profiles. Orange lines represent the traced rift axis, while yellow lines show where the topographic transects/profiles end. Map images from ACT-REACT Quickmap.

nonspreading regime we modeled. Devana and Rona Chasmata have the topographic profiles of full graben, supported by previous studies that studied their photogeology (e.g., E. R. Stofan et al. 1989; W. S. Kiefer & L. C. Swafford 2006; W. S. Kiefer et al. 2024). The segments between Atla and Themis Regios (Parga Chasmata) exhibit lower differences in elevation but show the same tendency for half-grabens along certain segments, though full grabens are more common. This is consistent with previous structural interpretations of Venus's rift architecture (e.g., W. S. Kiefer & L. C. Swafford 2004). However, this section was difficult to interpret with our method because of the structural complexity along the strike. Previous work has identified it as an older rift system overprinted by secondary corona formation (S. E. Smrekar et al. 2010) and subsequent extensional and volcanic phases (J. R. Graff et al. 2018). In the segment of Parga that was structurally consistent enough along the strike to average out, the pseudospreading regime does not replicate the observed topography of this major rift system. Similarly, the chasmata between Artemis Corona and Atla Regio are interacting with rift-embedded coronae, and the troughs that form those coronae's boundaries have identical profiles as half-grabens. Between the coronae, however, individual rift segments appear to be full grabens or are too complex to interpret with confidence.

While the pseudospreading models fail to explain the topography and morphology of the vast majority of chasmata on Venus, there are exceptions that highlight how those chasmata that may be examples of seafloor spreading are not representative of most rift settings on Venus. Britomartis Chasma's axial ridges and valleys, along with apparent transform faults, are consistent with the hypothesis that a seafloor-spreading-like system has developed within Artemis Corona. Artemis, along with other large coronae such as Quetzalpetlatl and Atahensik (Latona in older literature), is regarded as a possible site of subduction and trench rollback (e.g., D. McKenzie et al. 1992; D. T. Sandwell & G. Schubert 1992; G. Schubert & D. T. Sandwell 1995; A. Davaille et al. 2017; R. C. Ghail et al. 2024). That makes Artemis unique in that slab pull may be creating the unusually strong tectonic forces necessary for lithospheric rupture and seafloor spreading (D. Forsyth & S. Uyeda 1975). Therefore, while a spreading center may be active within Artemis Corona, this tectonic environment is not representative of rifting on Venus as a whole.

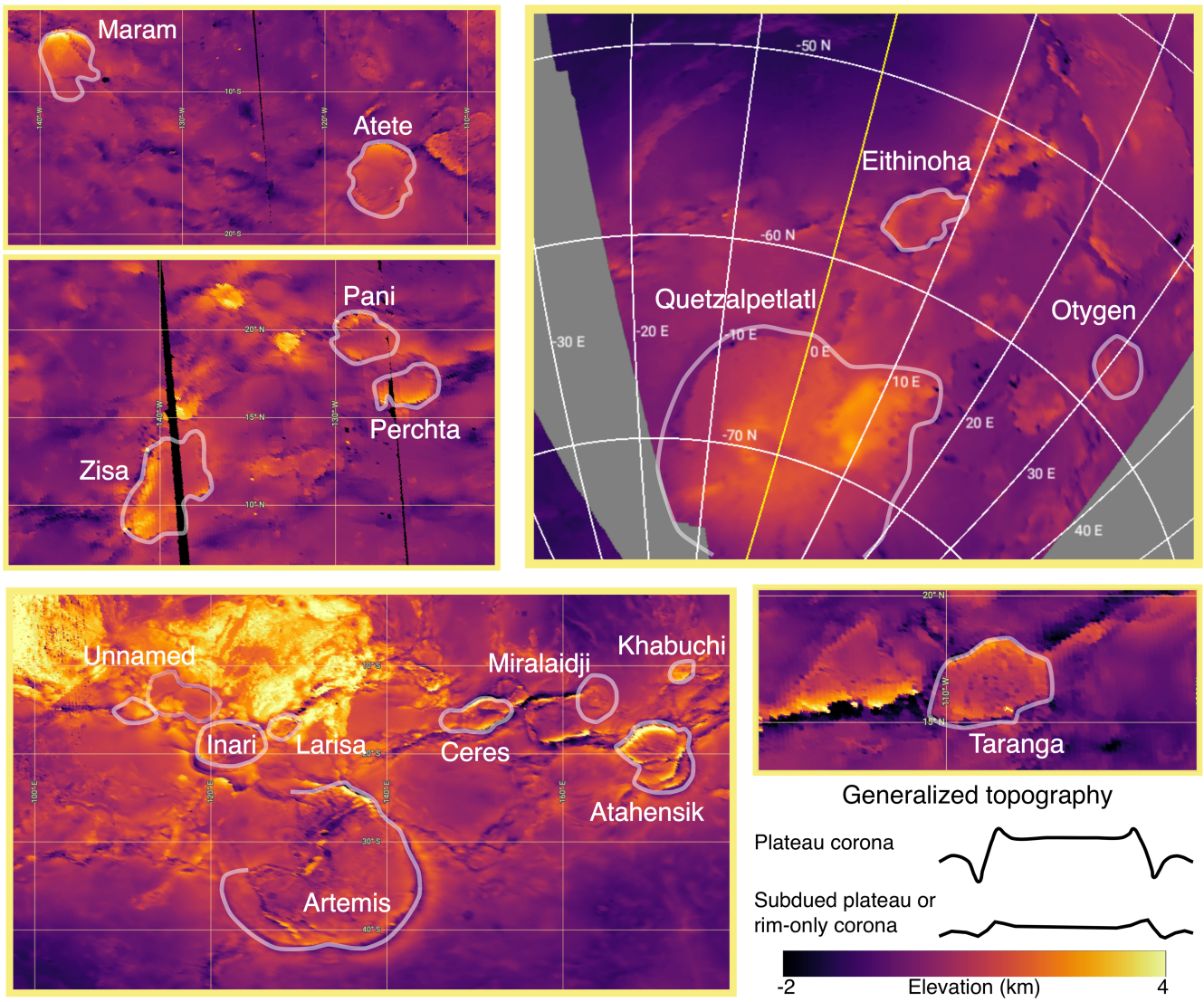

Figure 10. Each panel shows a region of the GRN with the associated rift-embedded coronae outlined and labeled. Rift-embedded coronae are irregular or polygonal features with raised interiors and troughs/rift segments that both form corona boundaries and grade into the regional rift system. The bottom right panel shows schematic generalizations of the two kinds of topographic profiles across rift-embedded coronae. Images from ACT-REACT Quickmap.

5. Conclusion

Based on comparisons between our numerical modeling experiments and the topography of individual rift segments along the GRN, we conclude that the GRN is not an MOR analog. While magmatism may be occurring along these rifts, they are not forming new crust along spreading centers. We find that, even under Venusian conditions, spreading centers on Venus would have similar features to spreading centers on Earth. This is typified by the apparent back-arc spreading within Artemis Corona. Instead, the GRN shares characteristics with continental rifting on Earth, exhibiting <100 km of extension, the formation of grabens and half-grabens, and linkages between separate rift segments.

In contrast, overthickening models readily explain key features of rift-embedded coronae. Based on the dynamics of our numerical modeling experiments and their similarity with the topography observed at Atahensik, Atete, Taranga, and Miralaidji Coronae, lithospheric dripping and high-density phase changes may be important formation processes for this class of coronae. Their positions along major segments of the GRN and between large mantle plumes suggest that excess volcanism and magmatism from mantle hot spots may cause regional formation and recycling of the crust in line with previous literature (e.g., A. Davaille et al. 2017; A. J. Gülcher et al. 2020).

This kind of regionalized hot-spot and rifting-dominated tectonism may point toward a tectonic mode that is dominated by upwellings from the mantle on Venus, in contrast to slab-pull-dominated plate tectonics on Earth. It is also consistent with aspects of globally fragmented (P. K. Byrne et al. 2021), plutonic-squishy (D. L. Lourenço et al. 2020), and deformable lid (J. Tian et al. 2023) geodynamic regimes. While the GRN does not represent a plate boundary, it may represent a diffuse zone of extension caused by mantle plumes stretching from the BAT to Artemis to Quetzalpetlatl. Within this zone, fragments of lithosphere (<1000 km across) have some horizontal mobility because of regional subduction and delamination that causes trench rollback (e.g., Artemis). This places convergent, divergent, transcurrent, and transform boundaries in relative proximity to each other and suggests that small-scale convection and crustal recycling occur locally along the

lithosphere–asthenosphere boundary instead of as a part of a system of global recycling as in plate tectonics. Modeling results also highlight the nuances of high-density phase changes on Venus versus Earth and how that difference may be expressed tectonically. The combination of reduced lithostatic pressure, an elevated geotherm, a thicker basalt crust, and an anhydrous lithosphere serves to "flip" the role of high-density phases in geodynamics. On Earth, eclogitization is a key process driving subduction (e.g., D. Forsyth & S. Uyeda 1975; C. P. Conrad & C. Lithgow-Bertelloni 2004; W. P. Schellart 2004), but on Venus, similar phase changes play an important role during **c**orona and hot-spot evolution, leading to a tectonic mode that does not exist on the modern Earth (e.g., A. J. Gülcher et al. 2020; D. L. Lourenço et al. 2020; J. Chen et al. 2022).

Acknowledgments

This work was supported by the University of Texas Institute for Geophysics and would not have been possible without the support of their researchers and staff. We would also like to thank Harm van Avendonk, Marce Hesse, and Othmar Müntener for their comments and contributions to the final draft of this paper. Additionally, discussions with Anna Gülcher, Paul Byrne, Scott King, Walter Kiefer, Matt Weller, Sue Smrekar, and others helped to enrich this work.

Supporting Data

The data and code used in this project are available through the Zenodo repository at doi:10.5281/zenodo.13175452 or through personal communication.

Appendix

As described in Section 2.3, we divide rift segments into five categories based on their morphology: "graben2" and "half-graben" which are analogs of the nonspreading model regime, "spreading" which is analogous to the pseudospreading model regime, "overthickening" which is analogous to the overthickening model regime, and "noisy/complex" which cannot be easily categorized (Table A1).

Model Animations

Movie 1. Animation showing the phase evolution of case 1. The initial parameters for this model are an extension rate of 0.01 cm yr^{-1}, a surface heat flux of 50 mW m^{-2}, and a crustal addition rate of 0.01 cm yr^{-1}.

Movie 2. Animation showing the phase evolution of case 2. The initial parameters for this model are an extension rate of 0.1 cm yr^{-1}, a surface heat flux of 50 mW m^{-2}, and a crustal addition rate of 0.01 cm yr^{-1}.

Movie 3. Animation showing the phase evolution of case 3. The initial parameters for this model are an extension rate of 1 cm yr^{-1}, a surface heat flux of 50 mW m^{-2}, and a crustal addition rate of 0.01 cm yr^{-1}.

Movie 4. Animation showing the phase evolution of case 4. The initial parameters for this model are an extension rate of 0.01 cm yr^{-1}, a surface heat flux of 80 mW m^{-2}, and a crustal addition rate of 0.01 cm yr^{-1}.

Movie 5. Animation showing the phase evolution of case 5. The initial parameters for this model are an extension rate of 0.1 cm yr^{-1}, a surface heat flux of 80 mW m^{-2}, and a crustal addition rate of 0.01 cm yr^{-1}.

Movie 6. Animation showing the phase evolution of case 6. The initial parameters for this model are an extension rate of 1 cm yr^{-1}, a surface heat flux of 80 mW m^{-2}, and a crustal addition rate of 0.01 cm yr^{-1}.

Movie 7. Animation showing the phase evolution of case 7. The initial parameters for this model are an extension rate of 0.01 cm yr^{-1}, a surface heat flux of 50 mW m^{-2}, and a crustal addition rate of 0.1 cm yr^{-1}.

Movie 8. Animation showing the phase evolution of case 8. The initial parameters for this model are an extension rate of 0.1 cm yr^{-1}, a surface heat flux of 50 mW m^{-2}, and a crustal addition rate of 0.1 cm yr^{-1}.

Movie 9. Animation showing the phase evolution of case 9. The initial parameters for this model are an extension rate of 1 cm yr^{-1}, a surface heat flux of 50 mW m^{-2}, and a crustal addition rate of 0.1 cm yr^{-1}.

Movie 10. Animation showing the phase evolution of case 10. The initial parameters for this model are an extension rate of 0.01 cm yr^{-1}, a surface heat flux of 80 mW m^{-2}, and a crustal addition rate of 0.1 cm yr^{-1}.

Movie 11. Animation showing the phase evolution of case 11. The initial parameters for this model are an extension rate of 0.01 cm yr^{-1}, a surface heat flux of 80 mW m^{-2}, and a crustal addition rate of 0.1 cm yr^{-1}.

Movie 12. Animation showing the phase evolution of case 12. The initial parameters for this model are an extension rate of 1 cm yr^{-1}, a surface heat flux of 80 mW m^{-2}, and a crustal addition rate of 0.1 cm yr^{-1}.

Movie 13. Animation showing the phase evolution of case 13. The initial parameters for this model are an extension rate of 0.01 cm yr^{-1}, a surface heat flux of 50 mW m^{-2}, and a crustal addition rate of 1 cm yr^{-1}.

Movie 14. Animation showing the phase evolution of case 14. The initial parameters for this model are an extension rate of 0.1 cm yr^{-1}, a surface heat flux of 50 mW m^{-2}, and a crustal addition rate of 1 cm yr^{-1}.

Movie 15. Animation showing the phase evolution of case 15. The initial parameters for this model are an extension rate of 1 cm yr^{-1}, a surface heat flux of 50 mW m^{-2}, and a crustal addition rate of 1 cm yr^{-1}.

Movie 16. Animation showing the phase evolution of case 16. The initial parameters for this model are an extension rate of 0.01 cm yr^{-1}, a surface heat flux of 80 mW m^{-2}, and a crustal addition rate of 1 cm yr^{-1}.

Movie 17. Animation showing the phase evolution of case 17. The initial parameters for this model are an extension rate of 0.1 cm yr^{-1}, a surface heat flux of 80 mW m^{-2}, and a crustal addition rate of 1 cm yr^{-1}.

Movie 18. Animation showing the phase evolution of case 18. The initial parameters for this model are an extension rate of 1 cm yr^{-1}, a surface heat flux of 80 mW m^{-2}, and a crustal addition rate of 1 cm yr^{-1}.

Table A1
Chasmata Analysis

Rift Segments	Graben	Half-graben	Spreading	Overthickening	Noisy/Complex	Diagnostic Features	Comments
Atahensik1[b]	…	…	…	X	…	Bowled plateau, high rims, surrounding trenches	…
Atete1[b]	…	…	…	X	…	Bowled plateau, high rims, surrounding trenches	…
Atete2[b]	…	…	…	X	…	Bowled plateau, high rims, surrounding trenches	…
BritomartisNorth	…	…	X	…	…	Axial ridge, off-axis depressions, wide rift/distant epaulements	…
BritomartisCentral	…	…	X	…	…	Axial ridge, off-axis depressions, wide rift/distant epaulements	Too short to interpret with confidence, influenced by adjacent transform faults
BritomartisSouth	…	…	X	…	…	Axial valley, off-axis ridges, surrounding plains at same depth as valley floor	…
CircumBonnevie1	…	…	X	…	…	Axial ridge, off-axis depressions	…
CircumBonnevie2	…	…	X	…	…	Axial ridge, off-axis depressions	Axial ridge disappears to the northwest, possible interaction with nearby transcurrent or transform faults
Dali1	X	…	…	…	…	One prominent epaulement, one subdued epaulement, deep and flat rift floor	…
Dali2[a]	X	…	…	…	…	Two prominent epaulements, deep and flat rift floor	Probable parallel boundary faults resulting in a third, smaller epaulement within the rift
Dali3[a]	…	X	…	…	…	One prominent epaulement, deep rift floor	…
Dali4	…	…	…	…	X	…	Too much complexity to interpret with confidence
Dali5	…	X	…	…	…	One prominent epaulement, deep rift floor	
DevanaNorth1	X	…	…	…	…	Two prominent epaulements, deep rift floor	Rift is elevated relative to background because it is located atop Beta Regio volcanic plateau
DevanaNorth2	X	…	…	…	…	Two prominent epaulements, deep rift floor	Rift is elevated relative to background because it is located atop Beta Regio volcanic plateau
DevanaNorth3	…	…	X	…	…	Axial valley, off-axis ridges, surrounding plains at same depth as valley floor	Rift is elevated relative to background because it is located atop Beta Regio volcanic plateau
DevanaSouth1	…	X	…	…	…	One prominent epaulement, deep rift floor	Rift is slightly relative to background because it is located south of Beta Regio volcanic plateau
DevanaSouth2	X	…	…	…	…	Two prominent epaulements, deep and flat rift floor	…
Diana1	X	…	…	…	…	Two prominent epaulements, deep rift floor	Narrow compared to other graben on Venus
Diana2	X	…	…	…	…	Two prominent epaulements, shallow but broad rift floor	…
Diana3[a]	…	X	…	…	…	Two prominent epaulements, deep rift floor	Could also be interpreted as a large half-graben but for the two prominent epaulements
Diana4[a]	…	X	…	…	…	One prominent epaulement, deep rift floor	…
Diana5[a]	…	X	…	…	…	One prominent epaulement, deep rift floor	…
Ganis1	…	…	…	…	X	…	Too much complexity to interpret with confidence
Ganis2	…	…	…	…	X	…	Too much complexity to interpret with confidence
Ganis3	…	…	…	…	X	…	Too much complexity to interpret with confidence
Hecate1	…	X	…	…	…	One prominent epaulement, deep, sloping rift floor	…
Hecate2	…	X	…	…	…	One prominent epaulement, deep, sloping rift floor	…
Juno1	…	…	…	…	X	…	Too much complexity to interpret with confidence
Juno2	…	…	…	…	X	…	Too much complexity to interpret with confidence
Latona	X	…	…	…	…	One prominent epaulement, one subdued epaulement, shallow yet broad rift floor	…
Miralaidji[b]	…	…	…	X	…	Slightly bowled plateau, low rims, central peak, shallow trench	…
Parga1	X	…	…	…	…	Two prominent epaulements, shallow but broad rift floor	Significant widening of the rift along the strike
Parga2	…	…	…	…	X	…	Possibly two half-grabens with a small rift-embedded corona developing in between, too much complexity to interpret with confidence

Table A1
(Continued)

Rift Segments	Graben	Half-graben	Spreading	Overthickening	Noisy/Complex	Diagnostic Features	Comments
Parga3	…	…	…	…	X	…	Too much complexity to interpret with confidence
Parga4	…	X	…	…	…	One prominent epaulement	Two segments with the same vergence
Parga5[a]	…	X	…	…	…	One prominent epaulement	…
Parga6	X	…	…	…	…	Two subdued epaulements, shallow yet broad rift floor	Small shield volcano complicates interpretation
Parga7	X	…	…	…	…	Two subdued epaulements, deep rift floor	Small shield volcano complicates interpretation
Parga8	…	…	…	…	X	…	Possibly a full graben rift or linked half-grabens but overprinted by subsequent volcanism and tectonism, too much complexity to interpret with confidence
Parga9	…	X	…	…	…	One prominent epaulement	Appears heavily degraded or overprinted by subsequent tectonism and volcanism
Quilla1	X	…	…	…	…	Two prominent epaulements, shallow but broad rift floor	…
Quilla2	…	X	…	…	…	One prominent epaulement, deep rift floor	Significant widening and deeping of the rift along the strike
Quilla3	X	…	…	…	…	Two prominent epaulements, deep rift floor	…
RalkUmgu	X	…	…	…	…	Two prominent epaulements, deep rift floor	Appears heavily degraded or overprinted by subsequent tectonism and volcanism
Rona1	X	…	…	…	…	One prominent epaulement	…
Rona2	X	…	…	…	…	Two subdued epaulements, wide and flat rift floor	Overprinted by volcanism, interference from preexisting topography
SouthAtla1	X	…	…	…	…	Two prominent epaulements, deep rift floor	…
SouthAtla2	…	X	…	…	…	One prominent epaulement, deep, sloping rift floor	…
SouthAtla3	X	…	…	…	…	Two prominent epaulements, deep rift floor	Likely two rift segments, a half-graben and a full graben
SouthAtla4	…	…	…	…	X	…	Too much complexity to interpret with confidence
Taranga[b]	…	…	…	X	…	Bowled plateau, high rims, surrounding trenches	…
Virava	X	…	…	…	…	Two subdued epaulements, deep rift floor	Appears heavily degraded or overprinted by subsequent tectonism and volcanism
Zewana	…	…	…	…	X	…	Appears heavily degraded or overprinted by subsequent tectonism and volcanism, too much complexity to interpret with confidence
Zverine	…	…	…	…	X	…	Overprinted by volcanism, interference from preexisting topography

Notes. This table describes the characterization of each rift segment, using the name of the .csv files in the data repository which trace out the rift axis across which profiles are drawn (each file consists of four columns: Distance (kilometers), Longitude, Latitude, and Venus Magellan Elevation (meters)). We divide the chasmata or coronae into five categories depending on which model regime they most closely resemble. "Graben" and "half-graben" are morphologically similar to the modeled nonspreading regime, while "spreading" and "overthickening" refer to the pseudospreading and overthickening regimes, respectively. "Noisy/complex" is a bin into which any chasma or corona that is does not resemble any of the model regimes because it has been subsequently degraded by volcanic or tectonic processes or because its morphology is too complex to interpret with confidence. The "diagnostic features" column contains descriptions of the chasma or corona morphology that informed their categorization, and "comments" contains any miscellaneous yet relevant observations, speculation, or explanation.

[a] Part of a corona's edge.

[b] Rift-embedded corona.

ORCID iDs

Nicholas J. Montiel https://orcid.org/0000-0002-2102-6651
Douglas J. Hemingway https://orcid.org/0000-0001-5617-207X

References

Airey, M. W., Mather, T. A., Pyle, D. M., & Ghail, R. C. 2017, The Distribution of Volcanism in the Beta-Atla-Themis Region of Venus: Its Relationship to Rifting and Implications for Global Tectonic Regimes, JGRE, 122, 1626
Anderson, F. S., & Smrekar, S. E. 2006, Global Mapping of Crustal and Lithospheric Thickness on Venus, JGRE, 111, E08006
Basilevsky, A. T. 1992, Global Tectonic Style, in Venus Geology, Geochemistry, and Geophysics: Research Results from the USSR, ed. V. L. Barsukov et al. (Tucson: Univ. of Arizona Press), 140
Bindschadler, D. L. 1995, Magellan: A New View of Venus' Geology and Geophysics, RvGeo, 33, 459
Buck, W. R., Lavier, L. L., & Poliakov, A. N. 2005, Modes of Faulting at Mid-Ocean Ridges, Natur, 434, 719
Byrne, P. K., Ghail, R. C., Şengör, A. M. C., et al. 2021, A Globally Fragmented and Mobile Lithosphere on Venus, PNAS, 118, e2025919118
Chen, J., Jiang, H., Tang, M., et al. 2022, Venus' Light Slab Hinders Its Development of Planetary-Scale Subduction, NatCo, 13, 7647
Conrad, C. P., & Lithgow-Bertelloni, C. 2004, The Temporal Evolution of Plate Driving Forces: Importance of "Slab Suction" versus "Slab Pull" During the Cenozoic, JGRB, 109, B10407
Crumpler, L. S., Head, J. W., & Aubele, J. C. 1993, Regional Mantle Upwelling on Venus: The Beta-Atla-Themis Anomaly and Correlation with Global Tectonic Patterns, LPSC, 24, 367
Cundall, P. A. 1987, Distinct Element Models, of Rock and Soil Structure, in Analytical and Computational Method in Engineering Rock Mechanics, ed. E. T. Brown (London: Allen & Unwin), 129
Davaille, A., Smrekar, S. E., & Tomlinson, S. 2017, Experimental and Observational Evidence for Plume-Induced Subduction on Venus, NatGe, 10, 349
Davies, J. H. 2013, Global Map of Solid Earth Surface Heat Flow, GGG, 14, 4608
Duesterhoeft, E., Quinteros, J., Oberhänsli, R., Bousquet, R., & de Capitani, C. 2014, Relative Impact of Mantle Densification and Eclogitization of Slabs on Subduction Dynamics: A Numerical Thermodynamic/Thermokinematic Investigation of Metamorphic Density Evolution, Tectp, 637, 20
Earle, S. 2019, Metamorphism and Metamorphic Rocks, Physical Geology (2nd ed.; Victoria, BC: BCcampus) https://opentextbc.ca/physicalgeology2ed/
Forsyth, D., & Uyeda, S. 1975, On the Relative Importance of the Driving Forces of Plate Motion, GeoJI, 43, 163
Foster, A., & Nimmo, F. 1996, Comparisons between the Rift Systems of East Africa, Earth and Beta Regio, Venus, E&PSL, 143, 183
Ghail, R. 2015, Rheological and Petrological Implications for a Stagnant Lid Regime on Venus, P&SS, 113, 2
Ghail, R. C., Smrekar, S. E., Widemann, T., et al. 2024, Volcanic and Tectonic Constraints on the Evolution of Venus, SSRv, 220, 36
Gmerek, A. T., Weller, M. B., Kiefer, W. S., & Gregg, T. K. P. 2024, Mapping and Analysis of Ganis Chasma Rift System, Atla Regio, Venus, LPICo, 3040, 1623
Graff, J. R., Ernst, R. E., & Samson, C. 2018, Evidence for Triple-Junction Rifting Focussed on Local Magmatic Centres Along Parga Chasma, Venus, Icar, 306, 122
Grimm, R. E. 1994, Recent Deformation Rates on Venus, JGR, 99, 23163
Guest, J. E., & Stofan, E. R. 1999, A New View of the Stratigraphic History of Venus, Icar, 139, 55
Gülcher, A. J., Gerya, T. V., Montési, L. G., & Munch, J. 2020, Corona Structures Driven by Plume–Lithosphere Interactions and Evidence for Ongoing Plume Activity on Venus, NatGe, 13, 547
Gülcher, A. J., Yu, T. Y., & Gerya, T. V. 2023, Tectono-Magmatic Evolution of Asymmetric Coronae on Venus: Topographic Classification and 3D Thermo-Mechanical Modeling, JGRE, 128, e2023JE007978
Gülcher, A. J. P., Gurnis, M., & Smrekar, S. E. 2024, The Peculiar Case of Rift Tectonics on Venus: 3D Models of Rift Interactions with Thermal Plumes and Crustal Intrusions, LPSC, 3040, 1425
Hanmer, S. 2023, Basic Structural Geology of Venus: A Review of the Gaps and How to Bridge Them, ESRv, 237, 104331
Harley, S. L. 1998, On the Occurrence and Characterization of Ultrahigh-temperature Crustal Metamorphism, GSLSP, 138, 81
Herrick, R. R., Bjonnes, E. T., Carter, L. M., et al. 2023, Resurfacing History and Volcanic Activity of Venus, SSRv, 219, 29
Herrick, R. R., & Hensley, S. 2023, Surface Changes Observed on a Venusian Volcano During the Magellan Mission, Sci, 379, 1205
Huismans, R. S., Buiter, S. J. H., & Beaumont, C. 2005, Effect of Plastic-viscous Layering and Strain Softening on Mode Selection During Lithospheric Extension, JGRB, 110, B02406
Jiménez-Díaz, A., Ruiz, J., Kirby, J. F., et al. 2015, Lithospheric Structure of Venus from Gravity and Topography, Icar, 260, 215
James, P. B., Zuber, M. T., & Phillips, R. J. 2013, Crustal Thickness and Support of Topography on Venus, JGRE, 118, 859
Ivanov, M. A., & Head, J. W. 2011, Global Geological Map of Venus, P&SS, 59, 1559
Kiefer, W. S., & Swafford, L. C. 2004, Rift System Architecture on Venus, LPSC, 35, 1607
Kiefer, W. S., & Swafford, L. C. 2006, Topographic Analysis of Devana Chasma, Venus: Implications for Rift System Segmentation and Propagation, JSG, 28, 2144
Kiefer, W. S., Weller, M. B., Gmerek, A. T., & Buck, W. R. 2024, Segmentation and Rift Basin Morphology in Central and Southern Devana Chasma, Venus: Full Graben, Half Graben, and Implications for Present-Day Tectonic Processes, LPICo, 3040, 1497
Krassilnikov, A. S., Kostama, V. P., Aittola, M., Guseva, E. N., & Cherkashina, O. S. 2012, Relationship of Coronae, Regional Plains and Rift Zones on Venus, P&SS, 68, 56
Lavier, L. L., & Buck, W. R. 2002, Half Graben Versus Large-offset Low-angle Normal Fault: Importance of Keeping Cool During Normal Faulting, JGRB, 107, 2122
Lavier, L. L., & Manatschal, G. 2006, A Mechanism to Thin the Continental Lithosphere at Magma-Poor Margins, Natur, 440, 324
Leech, M. L. 2001, Arrested Orogenic Development: Eclogitization, Delamination, and Tectonic Collapse, E&PSL, 185, 149
Lourenço, D. L. 2023, Estranged Planetary Twins, NatGe, 16, 2
Lourenço, D. L., Rozel, A. B., Ballmer, M. D., & Tackley, P. J. 2020, Plutonic-squishy Lid: A New Global Tectonic Regime Generated by Intrusive Magmatism on Earth-like Planets, GGG, 21, e08756
Maia, J. S., Wieczorek, M. A., & Plesa, A.-C. 2023, The Mantle Viscosity Structure of Venus, GeoRL, 50, e2023GL103847
Marcq, E., Bertaux, J. L., Montmessin, F., & Belyaev, D. 2013, Variations of Sulphur Dioxide at the Cloud Top of Venus's Dynamic Atmosphere, NatGe, 6, 25
McKenzie, D., Ford, P. G., Johnson, C., et al. 1992, Features on Venus Generated by Plate Boundary Processes, JGR, 97, 13533
Montiel, N. J., Masini, E., Lavier, L., Müntener, O., & Calassou, S. 2023, Mantle Deformation Processes During the Rift-to-drift Transition at Magma-poor Margins, GGG, 24, e2023GC010924
Müller, R. D., Roest, W. R., & Royer, J. Y. 1998, Asymmetric Sea-Floor Spreading Caused by Ridge–Plume Interactions, Natur, 396, 455
Mulyukova, E., & Bercovici, D. 2020, Mantle Convection in Terrestrial Planets, Oxford Research Encyclopedia of Planetary Science (Oxford: Oxford Press)
O'Rourke, J. G., & Smrekar, S. E. 2018, Signatures of Lithospheric Flexure and Elevated Heat Flow in Stereo Topography at Coronae on Venus, JGRE, 123, 369
Poliakov, A. N. B., Cundall, P. A., Podladchikov, Y. Y., & Lyakhovsky, V. A. 1993, An Explicit Inertial Method for the Simulation of Viscoelastic Flow: an Evaluation of Elastic Effects on Diapiric Flow in Two-and Three-layers Models, Flow and Creep in the Solar System: Observations, Modeling and Theory (Dordrecht: Springer), 175
Raimbourg, H., Jolivet, L., & Leroy, Y. 2007, Consequences of Progressive Eclogitization on Crustal Exhumation, a Mechanical Study, GeoJI, 168, 379
Reese, C. C., Solomatov, V. S., & Orth, C. P. 2007, Mechanisms for Cessation of Magmatic Resurfacing on Venus, JGRE, 112, E04S04
Regorda, A., Thieulot, C., van Zelst, I., et al. 2023, Rifting Venus: Insights from Numerical Modeling, JGRE, 128, e2022JE007588
Rosenblatt, P., Pinet, P. C., & Thouvenot, E. 1994, Comparative Hypsometric Analysis of Earth and Venus, GeoRL, 21, 465
Sandwell, D. T., & Schubert, G. 1992, Evidence for Retrograde Lithospheric Subduction on Venus, Sci, 257, 766
Schaber, G. G., Strom, R. G., Moore, H. J., et al. 1992, Geology and Distribution of Impact Craters on Venus: What Are They Telling Us?, JGR, 97, 13257
Schellart, W. P. 2004, Quantifying the Net Slab Pull Force as a Driving Mechanism for Plate Tectonics, GeoRL, 31, L07611
Schubert, G., & Sandwell, D. T. 1995, A Global Survey of Possible Subduction Sites on Venus, Icar, 117, 173

Searle, R. 2013, Mid-Ocean Ridges (Cambridge: Cambridge Univ. Press)
Shalygin, E. V., Markiewicz, W. J., Basilevsky, A. T., et al. 2015, Active Volcanism on Venus in the Ganiki Chasma Rift Zone, GeoRL, 42, 4762
Simons, M., Hager, B. H., & Solomon, S. C. 1994, Global Variations in the Geoid/Topography Admittance of Venus, Sci, 264, 798
Smrekar, S. E., Davaille, A., & Sotin, C. 2018, Venus Interior Structure and Dynamics, SSRv, 214, 88
Smrekar, S. E., Ostberg, C., & O'Rourke, J. G. 2023, Earth-like Lithospheric Thickness and Heat Flow on Venus Consistent with Active Rifting, NatGe, 16, 13
Smrekar, S. E., & Sotin, C. 2012, Constraints on Mantle Plumes on Venus: Implications for Volatile History, Icar, 217, 510
Smrekar, S. E., Stofan, E. R., Mueller, N., et al. 2010, Recent Hotspot Volcanism on Venus from VIRTIS Emissivity Data, Sci, 328, 605
Solomatov, V. S., & Moresi, L. N. 1996, Stagnant Lid Convection on Venus, JGR, 101, 4737
Stofan, E. R., Hamilton, V. E., Janes, D. M., & Smrekar, S. E. 1997, Coronae on Venus: Morphology and Origin, in Venus II: Geology, Geophysics, Atmosphere, and Solar Wind Environment, ed. S. W. Bougher, D. M. Hunten, R. J. Phillips et al. (Tucson, AZ: Univ. Arizona Press), 931
Stofan, E. R., Head, J. W., Campbell, D. B., et al. 1989, Geology of a Rift Zone on Venus: Beta Regio and Devana Chasma, GSAB, 101, 143
Stofan, E. R., & Smrekar, S. E. 2005, Large Topographic Rises, Coronae, Large Flow Fields, and Large Volcanoes on Venus: Evidence for Mantle Plumes?, in Plates, Plumes and Paradigms, ed. G. R. Foulger et al. (Boulder, CO: Geological Society of America)
Stoddard, P. R., & Jurdy, D. M. 2012, Topographic Comparisons of Uplift Features on Venus and Earth: Implications for Venus Tectonics, Icar, 217, 524
Strom, R. G., Schaber, G. G., & Dawson, D. D. 1994, The Global Resurfacing of Venus, JGR, 99, 10899
Svartman Dias, A. E., Lavier, L. L., & Hayman, N. W. 2015, Conjugate Rifted Margins Width and Asymmetry: The Interplay between Lithospheric Strength and Thermomechanical Processes, JGRB, 120, 8672
Taylor, S. R., & McLennan, S. 2008, Venus: A Twin Planet to Earth?, Planetary Crusts: Their Composition, Origin and Evolution (Cambridge: Cambridge Univ. Press), 181
Tian, J., Tackley, P. J., & Lourenço, D. L. 2023, The Tectonics and Volcanism of Venus: New Modes Facilitated by Realistic Crustal Rheology and Intrusive Magmatism, Icar, 399, 115539
Tsujimori, T., & Mattinson, C. 2021, Eclogites in Different Tectonic Settings, Encyclopedia of Geology (Amsterdam: Elsevier), 561
White, A. J. R. 1964, Clinopyroxenes from Eclogites and Basic Granulites, American Mineralogist: Journal of Earth and Planetary Materials, 49, 883
Wieczorek, M. A. 2015, Gravity and Topography of the Terrestrial Planets, in Treatise on Geophysics, ed. G. Schubert (2nd ed.; Amsterdam: Elsevier), 153
Zhang, J., & Green, H. W. 2007, Experimental Investigation of Eclogite Rheology and Its Fabrics at High Temperature and Pressure, JMetG, 25, 97